

Coupling-induced dynamics in a stochastic two-predator two-prey system with Markov switching

Ya-Nan Sun(孙雅楠), Xin-Zhi Liu(刘新芝), and You-Ming Lei(雷佑铭)
Citation: Chin. Phys. B, 2026, 35 (**8**): 080507. DOI: 10.1088/1674-1056/ae8daf
http://cpb.iphy.ac.cn; http://iopscience.iop.org/cpb

What follows is a list of articles you may be interested in

Statistical complexity and stochastic resonance in bistable coupled network systems excited by non-Gaussian noise

Meijuan He(何美娟), Lingyun Li(李凌云), Wantao Jia(贾万涛), and Jiangang Zhang(张建刚)
Chin. Phys. B, 2026, 35 (**3**): 030501. DOI: 10.1088/1674-1056/adfef7

An epidemiological stochastic predator-prey model with prey refuge and harvesting

Israr Ali, Hui Zhang(张慧), Syed Murad Ali Shah, Abdulwasea Alkhazzan, and Yassine Sabbar
Chin. Phys. B, 2026, 35 (**2**): 020503. DOI: 10.1088/1674-1056/adf17f

Dynamic balance and reliability of a stochastic ecosystem with Markov switching

Ya-Nan Sun(孙雅楠), Xin-Zhi Liu(刘新芝), and You-Ming Lei(雷佑铭)
Chin. Phys. B, 2026, 35 (**1**): 010507. DOI: 10.1088/1674-1056/adea58

Exploring clogging of interacting particles with hydrodynamic memory in a corrugated channel: A promising sensor of non-Brownian diffusion

Yuhui Luo(罗玉辉), Chunhua Zeng(曾春华), and Tao Huang(黄韬)
Chin. Phys. B, 2025, 34 (**8**): 080508. DOI: 10.1088/1674-1056/adecfc

Effects of potential field delay and coupling delay on collective behavior of a fractional-order coupled system in a dichotomous fluctuating potential

Yangfan Zhong(钟扬帆), Xi Chen(陈熙), Maokang Luo(罗懋康), and Tao Yu(蔚涛)
Chin. Phys. B, 2025, 34 (**5**): 050501. DOI: 10.1088/1674-1056/adbd15

Coupling-induced dynamics in a stochastic two-predator two-prey system with Markov switching

Ya-Nan Sun(孙雅楠)[1], Xin-Zhi Liu(刘新芝)[2], and You-Ming Lei(雷佑铭)[1,†]

[1] *School of Mathematics and Statistics, Northwestern Polytechnical University, Xi'an* 710072, *China*
[2] *Department of Applied Mathematics, University of Waterloo, Waterloo N2L* 3*G*1, *Ontario, Canada*

(Received 31 May 2026; revised manuscript received 14 July 2026; accepted manuscript online 21 July 2026)

We investigate a four-dimensional coupled predator–prey model that integrates white noise to model continuous environmental fluctuations and Markov switching to characterize discrete regime shifts. Compared with classical two-dimensional models, this formulation allows a more realistic description of complex multispecies interactions. In the deterministic case, the stability and bifurcation conditions for positive equilibrium are derived theoretically. The results show that increasing the coupling strength can induce Andronov–Hopf bifurcations and spiral dynamics, leading the system to evolve from a stable coexistence state to multimodal oscillations. In stochastic settings, the stochastic P-bifurcation phenomenon caused by noise and switching is identified through changes in the stationary probability density functions and the most probable trajectories. Based on the most probable trajectory theory, a quantitative indicator is further introduced to determine the bifurcation conditions in the switched system and to evaluate species coexistence in a switching environment. Results indicate that weak noise and switching rate can increase the coupling-induced bifurcation threshold and weaken multimodal oscillations. The combined influence of these factors provides a guiding basis for the coexistence of multiple species in switching environments.

Keywords: two-predator two-prey system, Markov switching, most probable trajectory

PACS: 05.40.–a, 02.50.–r

DOI: 10.1088/1674-1056/ae8daf **CSTR:** 32038.14.CPB.ae8daf

1. Introduction

Predator–prey models are widely used to describe population dynamics, but deterministic models often fail to capture real ecosystem dynamics under environmental fluctuations.[1,2] In fact, populations are affected not only by continuous small disturbances but also by regime shifts induced by seasonal alternations or human activities, which are commonly modeled as Markov switching.[3–5] This framework provides a more realistic description of sudden environmental changes and helps reveal the mechanisms underlying species persistence in heterogeneous environments.

In recent years, stochastic predator–prey models with Markov switching have been mainly studied in two-dimensional systems. Existing works have established sufficient conditions for weak persistence and extinction,[6,7] and analyzed stochastic P-bifurcations and equilibrium transitions using probability-weighted methods.[8–10] For models with general functional responses, explicit stability conditions for dynamical bifurcations have also been obtained.[11] Spatial extensions have further characterized persistence thresholds for reaction-diffusion systems under random switching.[12] However, two-dimensional models cannot adequately represent food web complexity with multiple predators and prey. Furthermore, the combined effects of multispecies coupling, white noise, and Markov switching in multidimensional ecosystems remain unclear. To address this limitation, two-predator two-prey systems provide a typical four-dimensional framework for describing interspecific competition and trophic interactions.

The theoretical study of two-predator two-prey coupled systems can be traced back to the classical resource competition model.[13] Early studies primarily examined stability and coexistence in deterministic systems, highlighting essential differences between single trophic-level stability and whole-system stability.[14] Later works developed the persistence theory of species and emphasized the roles of heteroclinic cycles and limit cycle oscillations.[15–17] In these models, coupling is a key mechanism for describing species interactions.[18,19] It is usually represented by predation and competition coefficients, which quantify interaction strengths among different trophic levels.[20] Existing studies have shown that coupling can affect pest control,[21] induce period-doubling and symmetry-breaking bifurcations,[22] destabilize otherwise stable subsystems through persistent antiphase oscillations,[23] and shape stability conditions and bifurcation behaviors through changes in coupling strength.[24]

However, most existing two-predator two-prey models are deterministic and insufficient to characterize the randomness and environmental switching in real ecosystems. Therefore, this work develops a four-dimensional stochastic ecological model incorporating Markov switching, white noise, and

†Corresponding author. E-mail: leiyouming@nwpu.edu.cn

© 2026 Chinese Physical Society and IOP Publishing Ltd. All rights, including for text and data mining, AI training, and similar technologies, are reserved.

coupling mechanisms. The model extends previous studies on coupling-induced oscillations and reveals the synergistic effects of switching, noise, and coupling. These effects generate rich dynamics, such as noise-delayed and switching-delayed bifurcations, coupling-induced spiral motion, and multimodal distributions, which provide theoretical insight into species coexistence in fluctuating environments.

This work makes three contributions. First, a four-dimensional coupled model with Markov switching and white noise is developed to extend conventional two-dimensional models and describe complex multispecies interactions. Second, coupling-induced bifurcations are analyzed under both deterministic and stochastic conditions, showing the transition from stable equilibria to multimodal oscillations. Third, the effects of noise intensity and switching rate on the critical coupling threshold are investigated, revealing how external disturbances and internal coupling jointly shape ecosystem stability.

The rest of this work is organized as follows. Section 2 formulates the two-predator two-prey model with white noise and Markov switching. Section 3 analyzes deterministic stability and coupling-induced oscillations. Section 4 extends the analysis to stochastic environments and examines the joint effects of noise, switching, and coupling on species coexistence. Section 5 presents the conclusions and future work.

2. Two-predator two-prey system

Based on MacArthur's pioneering work,[13] various models have been proposed to explore different ecosystems, as shown in Fig. 1. These differences mainly result from the varying interactions among species. For example, Figs. 1(a) and 1(b) assume competition either within a single trophic level (e.g., Y_1 and Y_2) or across two levels (e.g., X_1 and Y_2), while some others consider both simultaneously (Figs. 1(c)–1(e)).

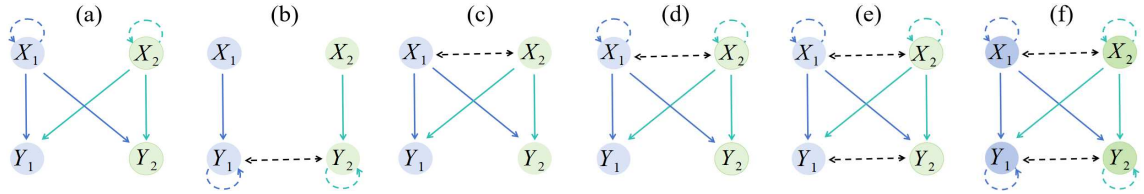


Fig. 1. Frameworks of the two-predator two-prey model. X_1 and X_2 denote prey populations, while Y_1 and Y_2 represent predator populations. Solid arrows are predation relationships, and dashed lines represent interference competition. (a) Refs. [13,25]; (b) Refs. [14,23]; (c) Refs. [26]; (d) Refs. [17,21,22]; (e) Refs. [24]; (f) present study.

Although these deterministic frameworks reveal complex population coexistence, randomness in natural environments is ignored. Therefore, we extend the deterministic framework (Fig. 1(e)) in Ref. [24] by incorporating more complex interactions and environmental disturbances. Specifically, the predator self-competition terms, continuous perturbations (Gaussian white noise), and discrete state transitions (Markov switching) are added. The resulting stochastic two-predator two-prey system with Markov switching is formulated as follows:

$$\begin{cases} \dot{X}_1 = a_1^{(r(t))}X_1 - b_{11}^{(r(t))}X_1^2 - b_{12}^{(r(t))}X_1X_2 - c_{11}^{(r(t))}X_1Y_1 - c_{12}^{(r(t))}X_1Y_2 + \sigma_1^{(r(t))}X_1W_1(t), \\ \dot{Y}_1 = -d_1^{(r(t))}Y_1 - h_1^{(r(t))}Y_1^2 + n_1^{(r(t))}c_{11}^{(r(t))}X_1Y_1 + \dfrac{\theta_1^{(r(t))}c_{21}^{(r(t))}}{m^{(r(t))}+X_2}X_2Y_1 - f_1^{(r(t))}Y_1Y_2 + \sigma_2^{(r(t))}Y_1W_2(t), \\ \dot{X}_2 = a_2^{(r(t))}X_2 - b_{22}^{(r(t))}X_2^2 - b_{21}^{(r(t))}X_1X_2 - \dfrac{c_{21}^{(r(t))}}{m^{(r(t))}+X_2}X_2Y_1 - c_{22}^{(r(t))}X_2Y_2 + \sigma_3^{(r(t))}X_2W_3(t), \\ \dot{Y}_2 = -d_2^{(r(t))}Y_2 - h_2^{(r(t))}Y_2^2 + n_2^{(r(t))}c_{12}^{(r(t))}X_1Y_2 + \theta_2^{(r(t))}c_{22}^{(r(t))}X_2Y_2 - f_2^{(r(t))}Y_1Y_2 + \sigma_4^{(r(t))}Y_2W_4(t), \end{cases} \tag{1}$$

where $X_1(t)$, $X_2(t)$ denote the small-sized and large-sized prey populations, and $Y_1(t)$, $Y_2(t)$ represent the small-sized and large-sized predator populations, respectively. The system (1) is considered with positive initial conditions $X_1(t_0) > 0$, $Y_1(t_0) > 0$, $X_2(t_0) > 0$, and $Y_2(t_0) > 0$. The parameters a_k (intrinsic growth rates), b_{kl} (inter-prey competition rate), c_{kl} (interspecies capture rate), d_k (predator mortality rate), n_k (consumption rate of prey x_1), h_k (predator self-competition rate), m (half saturation constant), f_k (inter-predator competition rate), and θ_k (consumption rate of prey x_2) for $k,l = 1,2$ are positive constants. $W_i(t)$ $(i = 1,2,3,4)$ represent the independent Gaussian white noises in the Stratonovich sense. These noises have autocorrelation functions $E[W_i(t)W_i(t+\tau)] = \delta(\tau)$, where $\delta(t)$ is the Dirac delta function and σ_i are noise intensities. The superscript $(r(t))$ signifies that system parameters are modulated by the state of the Markov chain, reflecting the ecological variations across different environmental modes (e.g., seasonal cycles or habitat destruction). Let $r(t)$ be a right-continuous Markov chain taking values in the finite state space $\mathbb{S} = \{1,2,\ldots,N\}$. Specifically, for each state $r(t) = i \in \mathbb{S}$, the system parameters $a_k^{(i)}, b_{kl}^{(i)}, c_{kl}^{(i)}, d_k^{(i)}, n_k^{(i)}, h_k^{(i)}, m^{(i)}, f_k^{(i)}$, and $\theta_k^{(i)}$ for $k,l = 1,2$ are constants. $r(t)$ is governed by the

transition matrix $\Gamma = \{\gamma_{ij}\}$ for $i, j = 1, 2, \ldots, N$, and

$$P\{r(t+\Delta t) = j \mid r(t) = i\} = \begin{cases} \gamma_{ij}\Delta t + o(\Delta t), & j \neq i, \\ 1 + \gamma_{ii}\Delta t + o(\Delta t), & j = i, \end{cases} \tag{2}$$

where γ_{ij} denotes transition rates, and $\gamma_{ii} = -\sum_{j\neq i}\gamma_{ij}$. Suppose that the Markov chain $r(t)$ is irreducible, implying that any state is accessible from any other one. Therefore, in light of finite-state Markov theory, the ergodicity property is valid.[7]

3. Deterministic case

3.1. Existence and uniqueness of positive equilibrium

In the absence of Markov switching and white noise, the system (1) reduces to a deterministic one. After replacing the random variables X_1, Y_1, X_2, Y_2 with deterministic variables x_1, y_1, x_2, y_2, the equilibria of the deterministic non-switched system can be solved by nullclines, satisfying $\dot{x}_1 = \dot{y}_1 = \dot{x}_2 = \dot{y}_2 = 0$. Given our focus on a healthy food chain that sustains all four species, this work investigates how coupling strength, white noise, and Markov switching jointly influence multi-species coexistence on ecosystem stability. Therefore, our analysis is restricted to the dynamical behavior of the internal coexistence equilibrium $E(x_1^*, y_1^*, x_2^*, y_2^*)$. Specifically,

$$\begin{aligned} x_1^* &= M_2 - M_3 x_2^* - \frac{M_4 x_2^*}{m + x_2^*}, \\ y_1^* &= \frac{h_2\left(n_1 c_{11} x_1^* + \frac{\theta_1 c_{21} x_2^*}{m+x_2^*} - d_1\right) - f_1\left(n_2 c_{12} x_1^* + \theta_2 c_{22} x_2^* - d_2\right)}{h_1 h_2 - f_1 f_2}, \\ y_2^* &= \frac{h_1\left(n_2 c_{12} x_1^* + \theta_2 c_{22} x_2^* - d_2\right) - f_2\left(n_1 c_{11} x_1^* + \frac{\theta_1 c_{21} x_2^*}{m+x_2^*} - d_1\right)}{h_1 h_2 - f_1 f_2}. \end{aligned} \tag{3}$$

The values of x_2^* can be calculated by solving the following cubic equation:[24]

$$A_1 x_2^{*3} + A_2 x_2^{*2} + A_3 x_2^* + A_4 = 0, \tag{4}$$

where

$$\begin{aligned} &A_1 = N_4, \ \ A_2 = N_1 + 2mN_4 + N_2, \ \ A_3 = 2mN_1 + mN_2 + N_3 + m^2 N_4 + N_5, \ \ A_4 = m^2 N_1 + mN_3, \\ &M_1 = b_{11} + \frac{1}{h_1 h_2 - f_1 f_2}\left((c_{11}h_2 - c_{12}f_2)n_1 c_{11} + (c_{12}h_1 - c_{11}f_1)n_2 c_{12}\right), \\ &M_2 = \frac{a_1(h_1 h_2 - f_1 f_2) + (c_{11}h_2 - c_{12}f_2)d_1 + (c_{12}h_1 - c_{11}f_1)d_2}{M_1(h_1 h_2 - f_1 f_2)}, \\ &M_3 = \frac{b_{12}(h_1 h_2 - f_1 f_2) + (c_{12}h_1 - c_{11}f_1)\theta_2 c_{22}}{M_1(h_1 h_2 - f_1 f_2)}, \ \ M_4 = \frac{(c_{11}h_2 - c_{12}f_2)\theta_1 c_{21}}{M_1(h_1 h_2 - f_1 f_2)}, \\ &N_1 = a_2 - b_{21}M_2 + \frac{(d_2 h_1 - d_1 f_2)c_{22} + M_2 c_{22}(n_1 c_{11} f_2 - c_{12} h_1 n_2)}{h_1 h_2 - f_1 f_2}, \\ &N_2 = b_{21}M_4 + \frac{M_4 c_{22}(c_{12}h_1 n_2 - c_{11}f_2 n_1) + \theta_1 c_{21} f_2 c_{22}}{h_1 h_2 - f_1 f_2} + \frac{M_3 c_{21}(c_{11}h_2 n_1 - c_{12}f_1 n_2) + \theta_2 c_{21} f_1 c_{22}}{h_1 h_2 - f_1 f_2}, \\ &N_3 = \frac{c_{21}(d_1 h_2 - d_2 f_1 - M_2(h_2 c_{11} n_1 - n_2 c_{12} f_1))}{h_1 h_2 - f_1 f_2}, \quad N_5 = \frac{c_{21}\left((M_4 c_{11} n_1 - \theta_1 c_{21})h_2 - M_4 c_{12} f_1 n_2\right)}{h_1 h_2 - f_1 f_2}, \\ &N_4 = M_3\frac{((-c_{11}f_2 n_1 + c_{12}h_1 n_2)c_{22} + b_{21}(h_1 h_2 - f_1 f_2))}{h_1 h_2 - f_1 f_2} - \frac{h_1\theta_2 c_{22}^2 + b_{22}(h_1 h_2 - f_1 f_2)}{h_1 h_2 - f_1 f_2}. \end{aligned} \tag{5}$$

The cubic equation given by Eq. (4) has discriminant $\Delta = 18A_1A_2A_3A_4 - 4A_2^3A_4 + A_2^2A_3^2 - 4A_1A_3^3 - 27A_1^2A_4^2$. For $\Delta > 0$, it has three distinct real roots, and for $\Delta < 0$, one real root and a pair of imaginary roots. A unique positive solution x_2^* exists if $\Delta < 0$ and $A_1A_4 < 0$. Moreover, for the interior equilibrium $E^*(x_1^*, y_1^*, x_2^*, y_2^*)$ to be biologically meaningful, x_1^*, y_1^*, and y_2^* must be positive.

3.2. Local stability of positive equilibrium

Linearizing the deterministic part of system (1), we obtain the local asymptotic stability condition for its positive equilibrium E^* using the Jacobian matrix and Routh–Hurwitz criteria.[24,27] The characteristic equation of the deterministic non-switched system at the equilibrium E^* is given below:

$$\lambda^4 + B_1^*\lambda^3 + B_2^*\lambda^2 + B_3^*\lambda + B_4^* = 0. \tag{6}$$

The specific expressions of $B_i^*(i = 1, 2, 3, 4)$ are (see Appendix A)

$$B_1^* = B_1|_{E^*}, \quad B_2^* = B_2|_{E^*}, \quad B_3^* = B_3|_{E^*}, \quad B_4^* = B_4|_{E^*}, \tag{7}$$

where

$$\begin{aligned} B_1 &= -(J_{11} + J_{22} + J_{33} + J_{44}), \ \ B_4 = \det(J), \\ B_2 &= J_{11}(J_{22} + J_{33} + J_{44}) + J_{22}(J_{33} + J_{44}) + J_{33}J_{44} \\ &\quad - J_{12}J_{21} - J_{13}J_{31} - J_{14}J_{41} - J_{23}J_{32} - J_{24}J_{42} - J_{34}J_{43}, \end{aligned}$$

$$
\begin{aligned}
B_3 = & -(J_{11}J_{22}J_{33}+J_{11}J_{22}J_{44}+J_{11}J_{33}J_{44}+J_{22}J_{33}J_{44})\\
& +J_{11}J_{23}J_{32}+J_{11}J_{24}J_{42}+J_{11}J_{34}J_{43}+J_{22}J_{13}J_{31}\\
& +J_{22}J_{14}J_{41}+J_{22}J_{34}J_{43}+J_{33}J_{12}J_{21}+J_{33}J_{14}J_{41}\\
& +J_{33}J_{24}J_{42}+J_{44}J_{12}J_{21}+J_{44}J_{13}J_{31}+J_{44}J_{23}J_{32}\\
& -J_{12}J_{23}J_{31}-J_{12}J_{24}J_{41}-J_{13}J_{34}J_{41}-J_{23}J_{34}J_{42}\\
& -J_{13}J_{21}J_{32}+J_{13}J_{22}J_{31}-J_{14}J_{21}J_{42}+J_{14}J_{22}J_{41}\\
& -J_{14}J_{31}J_{43}-J_{24}J_{32}J_{43}, \qquad (8)
\end{aligned}
$$

with

$$
\begin{aligned}
& J_{11}=a_1-2b_{11}x_1-b_{12}x_2-c_{11}y_1-c_{12}y_2,\ \ J_{12}=-c_{11}x_1,\\
& J_{13}=-b_{12}x_1,\ \ J_{14}=-c_{12}x_1,\ \ J_{21}=n_1c_{11}y_1,\\
& J_{22}=-d_1-2h_1y_1+n_1c_{11}x_1+\frac{\theta_1c_{21}x_2}{m+x_2}-f_1y_2,\\
& J_{23}=\frac{\theta_1c_{21}my_1}{(m+x_2)^2},\ \ J_{24}=-f_1y_1,\ \ J_{31}=-b_{21}x_2,\\
& J_{32}=-\frac{c_{21}x_2}{m+x_2},\\
& J_{33}=a_2-2b_{22}x_2-b_{21}x_1-\frac{mc_{21}y_1}{(m+x_2)^2}-c_{22}y_2,\\
& J_{34}=-c_{22}x_2,\ \ J_{41}=n_2c_{12}y_2,\ \ J_{42}=-f_2y_2,\ \ J_{43}=\theta_2c_{22}y_2,\\
& J_{44}=-d_2-2h_2y_2+n_2c_{12}x_1+\theta_2c_{22}x_2-f_2y_1. \qquad (9)
\end{aligned}
$$

According to the Routh–Hurwitz criteria, E^* is locally asymptotically stable if[24]

$$B_1^*>0,\quad B_3^*>0,\quad \bar{B}^*=B_1^*B_2^*-B_3^*>0,$$

$$\hat{B}^*=B_1^*B_2^*B_3^*-B_3^{*2}-B_1^{*2}B_4^*>0. \qquad (10)$$

To validate the above conclusions, the time series of the deterministic non-switched system is presented in Fig. 2. The parameter values are[24] $a_1=0.85$, $a_2=0.7$, $b_{11}=1.4\times10^{-4}$, $b_{22}=3.5\times10^{-4}$, $c_{11}=0.013$, $c_{22}=0.03$, $m=1200$, $d_1=0.04$, $d_2=0.03$, $n_1=0.007$, $n_2=0.001$, $\theta_1=0.0104$, $\theta_2=0.0093$, $c_{12}=0.005$, $c_{21}=0.002$, $b_{12}=1\times10^{-6}$, $b_{21}=9\times10^{-4}$, $f_1=0.002$, $f_2=5\times10^{-4}$, $h_1=1.2\times10^{-5}$, $h_2=1\times10^{-5}$, and $\sigma_1=\sigma_2=\sigma_3=\sigma_4=0$. Substituting these values into Eq. (10) yields $B_1^*=0.15$, $B_3^*=2.52\times10^{-3}$, $\bar{B}^*=4.92\times10^{-3}$, and $\hat{B}^*=2.06\times10^{-6}$. Hence, the steady state of the system is confirmed to be a locally asymptotically stable equilibrium E^*.

In the absence of white noise and Markov switching, Fig. 2(a) displays three solution trajectories starting from initial points L_k, $(k=1,2,3)$, all converging to equilibrium E^*, indicating stable species coexistence. Figures 2(b) and 2(d) show the transient anti-phase oscillations between prey x_1 and predator y_1: As x_1 increases, y_1 decreases, forming repeated cycles until stabilization. Figure 2(c) exhibits impulse-like oscillations in prey x_2 without corresponding behavior in predator y_2. The asymmetry appears to originate in distinct functional responses between the predators. Both consume prey x_1 at a linear rate, and predator y_2 also feeds linearly on x_2. In contrast, predator y_1 responds to x_2 with a Holling type II saturating functional response. Therefore, even without random disturbances, multidimensional ecosystems can exhibit complex nonlinear behaviors.

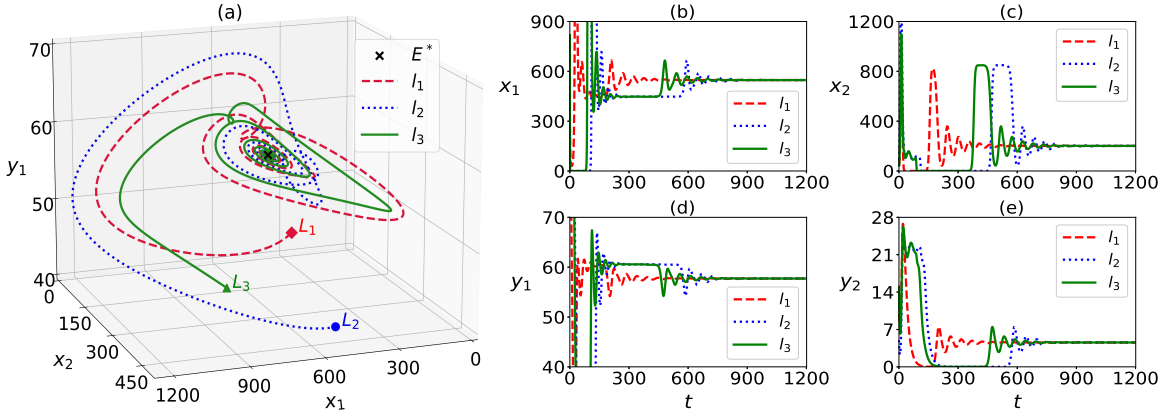


Fig. 2. Trajectories of the deterministic non-switched system starting from three initial values L_k $(k=1,2,3)$. The curves l_k represent the trajectories originating from L_k, which eventually converge to the interior equilibrium E^*. Specifically, $L_1=(350,45,100,10)$, $L_2=(450,40,400,5)$, $L_3=(850,45,350,15)$, and $E^*\approx(547.37,57.72,201.32,4.56)$.

3.3. Effects of coupling strength

Coupling between species is an important factor affecting species coexistence and ecosystem stability. We now examine the impact of coupling strength on the stability characteristics of the positive equilibrium E^*, which governs long-term coexistence dynamics. The coupling strength c_{21} serves as a critical control parameter, representing the predation rate of predator y_1 on prey x_2 and thus measuring interaction intensity. Based on the analysis in the previous subsection, the necessary and sufficient conditions for the existence of an Andronov–Hopf bifurcation at $c_{21}=c_{21}^*$ are[28]

$$
\begin{aligned}
& B_j^*(c_{21}^*)>0,\quad \bar{B}^*=B_1^*(c_{21}^*)B_2^*(c_{21}^*)-B_3^*(c_{21}^*)>0,\\
& B_\xi^*=\frac{\mathrm{d}\xi_j}{\mathrm{d}c_{21}}\Big|_{c_{21}=c_{21}^*}\neq0,\ \ j=1,2,3,4,\\
& \hat{B}^*=B_1^*(c_{21}^*)B_2^*(c_{21}^*)B_3^*(c_{21}^*)-B_3^{*2}(c_{21}^*)
\end{aligned}
$$

$$-B_1^{*2}(c_{21}^*)B_4^*(c_{21}^*)=0, \tag{11}$$

where ξ_j is the real part of the j-th eigenvalue, and $B_\xi^* \neq 0$ denotes the transversality condition essential for bifurcation occurrence. To elucidate these theoretical conditions, the bifurcation diagrams of the steady states y_1 and y_2 as functions of the coupling strength c_{21} are presented in Fig. 3.

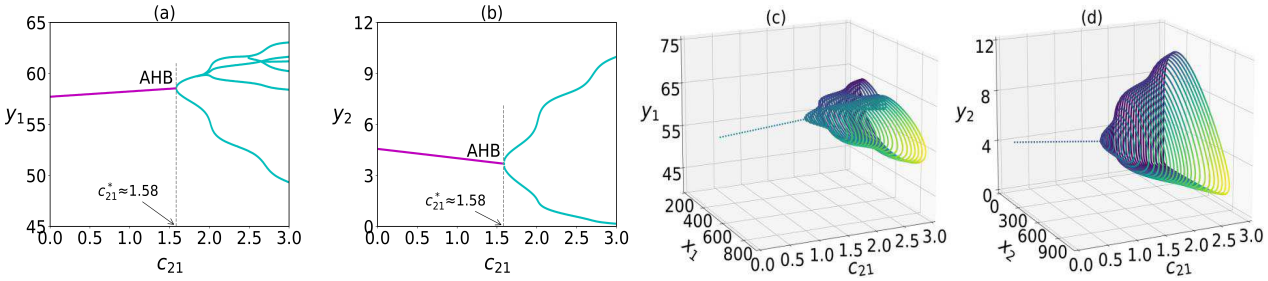


Fig. 3. Bifurcation diagrams of positive steady states in the deterministic non-switched system with varying coupling strength c_{21}. (a) and (b) Two-dimensional bifurcation diagrams of steady states y_1 and y_2 with respect to c_{21}, showing an Andronov–Hopf bifurcation (AHB) at $c_{21}=c_{21}^*\approx1.58$ (theoretically calculated). (c) and (d) Three-dimensional bifurcation diagrams of phase portraits x_1–y_1 and x_2–y_2 with respect to c_{21}.

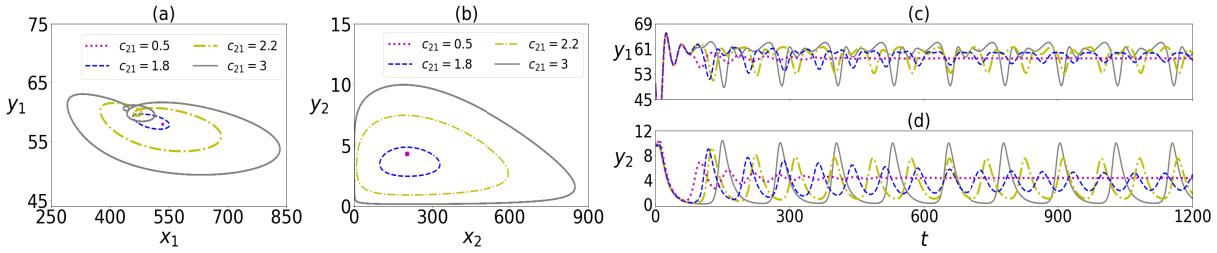


Fig. 4. Phase portraits and time series of the deterministic non-switched system under different coupling strengths c_{21}. Initial values are $(x_1(0),y_1(0),x_2(0),y_2(0))=(100,50,100,10)$. Increasing c_{21} will cause the steady state to change from an equilibrium to a limit cycle, or even result in a spiral trajectory.

Figure 3 presents the bifurcation analysis with respect to the coupling strength c_{21}, representing how intensifying predation pressure from predator y_1 on prey x_2 reshapes ecosystem dynamics. Figures 3(a) and 3(b) show the equilibrium and periodic branches for predator populations y_1 and y_2, respectively. An Andronov–Hopf bifurcation is identified at $c_{21}\approx1.58$, a value derived theoretically from Eqs. (9)–(11). Below this threshold, the system maintains a stable equilibrium where all species coexist. Above it, the system transitions to stable periodic oscillations. Biologically, stronger predation of y_1 on x_2 breaks the original trophic balance and redistributes energy flow among species, thereby amplifying population fluctuations. With further increases in c_{21}, the dynamics of the species pair (x_1,y_1) evolve from simple oscillations to more complex behaviors, including asymmetric oscillations (at $c_{21}\approx1.95$) and multimodal oscillations (for $c_{21}>2.51$).[28,29] This might be because the predator y_1 obtains resources from both x_1 and x_2, whereas the interaction involving x_2 is regulated by the Holling type II functional response. In contrast, the species pair (x_2,y_2) only undergoes the initial Andronov–Hopf bifurcation, without additional bifurcations, but shows declining population densities and heightened extinction risk. This may be because increasing c_{21} redirects part of the resource flow from x_2 to y_1, reducing the food supply for y_2. Thus, the species pair (x_2,y_2) mainly shifts to a limit cycle with lower population levels, rather than developing further complex bifurcations. Figures 3(c) and 3(d) provide three-dimensional confirmation of the complex bifurcation structure and cascading phenomenon.[22,29] The increasing oscillation amplitude and the emergence of spiral trajectories indicate that higher species richness amplifies ecosystem complexity, which may not be conducive to species coexistence.

To further analyze, we selected coupling strength values $c_{21}=0.5,1.8,2.2$ and 3 to represent distinct dynamical states identified in Fig. 3. The corresponding time series and phase portraits of the deterministic non-switched system are plotted in Fig. 4. For $c_{21}=0.5$, the steady state is an equilibrium, and the time series trajectory converges to a fixed point. At $c_{21}=1.8$, the steady state becomes a limit cycle, and the phase diagram shows a closed orbit. For $c_{21}=2.2$ and $c_{21}=3$, the phase diagram of species pair (x_1,y_1) exhibits spiral shapes of different sizes.[22,29] This self-intersection phenomenon in the 2D projection confirms the complex torsion of the trajectory in the four-dimensional phase space.[28] In contrast, the species pair (x_2,y_2) mainly exhibits enlarged oscillation amplitudes, while its phase portrait remains a stable limit cycle, as shown in Fig. 4(b). This asymmetric response indicates that as c_{21} increases, the predation pressure imposed by y_1 on x_2 becomes stronger, directly disturbing the population balance of the second predator–prey pair. The enlarged oscillation amplitude implies that the population density of (x_2,y_2) is more likely to approach low-density states during oscillations, thereby increasing its potential extinction risk. The time series

in Figs. 4(c) and 4(d) further validate the above conclusions.

4. Stochastic case

In this section, we investigate the influence of coupling strength on the system dynamics under the combined action of two random mechanisms: white noise and Markov switching. Following a similar analytical structure to the deterministic framework, we first establish the mathematical foundation by proving the existence and uniqueness of positive solutions for the stochastic system.

4.1. Existence and uniqueness of stochastic positive solution

Theorem 1 For any initial value $(X_1(0),Y_1(0),X_2(0),Y_2(0),r(0)) \in \mathbb{R}^4 \times \mathbb{S}$, there exists a unique positive solution $(X_1(t),Y_1(t),X_2(t),Y_2(t),r(t)) \in \mathbb{R}^4_+ \times \mathbb{S}$ to system (1) for all $t \geq 0$ with probability one.

Proof Apply the logarithmic transformation $q_1(t) = \ln X_1(t)$, $p_1(t) = \ln Y_1(t)$, $q_2(t) = \ln X_2(t)$, and $p_2(t) = \ln Y_2(t)$. By the Itô lemma, the system (1) is transformed into the following form for $t \geq 0$:[7,30]

$$\begin{cases} \mathrm{d}q_1 = \left(a_1^{(r(t))} - b_{11}^{(r(t))}\mathrm{e}^{q_1} - b_{12}^{(r(t))}\mathrm{e}^{q_2} - c_{11}^{(r(t))}\mathrm{e}^{p_1} - c_{12}^{(r(t))}\mathrm{e}^{p_2} + \frac{\sigma_1^{2(r(t))}}{2}\right)\mathrm{d}t + \sigma_1^{(r(t))}\mathrm{d}B_1(t), \\ \mathrm{d}p_1 = \left(-d_1^{(r(t))} - h_1^{(r(t))}\mathrm{e}^{p_1} + n_1^{(r(t))}c_{11}\mathrm{e}^{q_1} + \frac{\theta_1^{(r(t))}c_{21}^{(r(t))}}{m^{(r(t))}+\mathrm{e}^{q_2}}\mathrm{e}^{q_2} - f_1^{(r(t))}\mathrm{e}^{p_2} + \frac{\sigma_2^{2(r(t))}}{2}\right)\mathrm{d}t + \sigma_2^{(r(t))}\mathrm{d}B_2(t), \\ \mathrm{d}q_2 = \left(a_2^{(r(t))} - b_{22}^{(r(t))}\mathrm{e}^{q_2} - b_{21}^{(r(t))}\mathrm{e}^{q_1} - \frac{c_{21}^{(r(t))}}{m^{(r(t))}+\mathrm{e}^{q_2}}\mathrm{e}^{p_1} - c_{22}^{(r(t))}\mathrm{e}^{p_2} + \frac{\sigma_3^{2(r(t))}}{2}\right)\mathrm{d}t + \sigma_3^{(r(t))}\mathrm{d}B_3(t), \\ \mathrm{d}p_2 = \left(-d_2^{(r(t))} - h_2^{(r(t))}\mathrm{e}^{p_2} + n_2^{(r(t))}c_{12}\mathrm{e}^{q_1} + \theta_2^{(r(t))}c_{22}^{(r(t))}\mathrm{e}^{q_2} - f_2^{(r(t))}\mathrm{e}^{p_1} + \frac{\sigma_4^{2(r(t))}}{2}\right)\mathrm{d}t + \sigma_4^{(r(t))}\mathrm{d}B_4(t), \end{cases} \tag{12}$$

with initial values $(q_1(0),p_1(0),q_2(0),p_2(0)) = (\ln X_1(0),\ln Y_1(0),\ln X_2(0),\ln Y_2(0))$. $B_j(t)$ $(j = 1,2,3,4)$ are the Brownian motions defined on the complete probability space $(\Omega,\mathcal{F},\{\mathcal{F}_t\}_{t\geq 0},\mathbb{P})$. Since the coefficients of system (12) satisfy the local Lipschitz condition, there exists a unique local solution $(q_1(t),p_1(t),q_2(t),p_2(t),r(t)) \in \mathbb{R}^4 \times \mathbb{S}$ on $t \in [0,\tau_\mathrm{e})$ a.s., where τ_e is the explosion time. To show this solution is global, we prove $\tau_\mathrm{e} = \infty$ a.s. Let $\varepsilon_0 \geq 1$ be sufficiently large such that initial values lie within the interval $[1/\varepsilon_0,\varepsilon_0]$. For each integer $\varepsilon \geq \varepsilon_0$, define the stopping time as

$$\tau_\varepsilon = \inf\left\{t \in [0,\tau_\mathrm{e}) : \min\{X_1(t),Y_1(t),X_2(t),Y_2(t)\} \leq \frac{1}{\varepsilon} \right.$$
$$\left. \text{or } \max\{X_1(t),Y_1(t),X_2(t),Y_2(t)\} \geq \varepsilon\right\}. \tag{13}$$

Clearly, τ_ε increases as $\varepsilon \to \infty$. Let $\tau_\infty = \lim_{\varepsilon\to\infty}\tau_\varepsilon$, whence $\tau_\infty \leq \tau_\mathrm{e}$ a.s. If $\tau_\infty = \infty$ a.s. is true, then $\tau_\mathrm{e} = \infty$ and $(X_1(t),Y_1(t),X_2(t),Y_2(t)) \in \mathbb{R}^4_+$ a.s. for all $t \geq 0$. Consequently, to complete the proof, it suffices to prove $\tau_\infty = \infty$ a.s. Suppose, for contradiction, that this does not hold; then there exist constants $T > 0$ and $\xi \in (0,1)$ for which

$$\mathbb{P}\{\tau_\infty \leq T\} > \xi. \tag{14}$$

Consequently, one can find an integer $\varepsilon_1 \geq \varepsilon_0$ satisfying

$$\mathbb{P}\{\tau_\varepsilon \leq T\} \geq \xi, \quad \forall \varepsilon \geq \varepsilon_1. \tag{15}$$

Define a C^2-function $V : \mathbb{R}^4_+ \to \bar{\mathbb{R}}_+$ by

$$\begin{aligned} V(X_1,Y_1,X_2,Y_2) = {} & \left(X_1 - \eta - \eta\ln\frac{X_1}{\eta}\right) \\ & + \psi_1(Y_1 - 1 - \ln Y_1) + \psi_2(X_2 - 1 - \ln X_2) \\ & + \psi_3(Y_2 - 1 - \ln Y_2), \end{aligned} \tag{16}$$

where η,ψ_1,ψ_2, and ψ_3 are the positive switching parameters to be determined later. The nonnegativity of the function V can be seen from $w - 1 - \ln w \geq 0$ for any $w > 0$.

According to the Itô lemma, a direct calculation of the differential $\mathrm{d}V(t)$ along the solutions leads to

$$\begin{aligned} \mathrm{d}V(X_1,Y_1,X_2,Y_2) = {} & \mathcal{L}V(X_1,Y_1,X_2,Y_2)\mathrm{d}t + \sigma_1^{(r(t))}(X_1 - \eta)\mathrm{d}B_1(t) + \sigma_2^{(r(t))}\psi_1(Y_1 - 1)\mathrm{d}B_2(t) \\ & + \sigma_3^{(r(t))}\psi_2(X_2 - 1)\mathrm{d}B_3(t) + \sigma_4^{(r(t))}\psi_3(Y_2 - 1)\mathrm{d}B_4(t), \end{aligned} \tag{17}$$

where $\mathcal{L}V : \mathbb{R}^4_+ \to \bar{\mathbb{R}}$ is defined by

$$\begin{aligned} \mathcal{L}V = {} & (X_1 - \eta)\left(a_1^{(r(t))} - b_{11}^{(r(t))}X_1 - b_{12}^{(r(t))}X_2 - c_{11}^{(r(t))}Y_1 - c_{12}^{(r(t))}Y_2\right) + \psi_1(Y_1 - 1)\left(-d_1^{(r(t))} - h_1^{(r(t))}Y_1 + n_1^{(r(t))}c_{11}^{(r(t))}X_1\right. \\ & \left. + \frac{\theta_1^{(r(t))}c_{21}^{(r(t))}X_2}{m^{(r(t))} + X_2} - f_1^{(r(t))}Y_2\right) + \psi_2(X_2 - 1)\left(a_2^{(r(t))} - b_{22}^{(r(t))}X_2 - b_{21}^{(r(t))}X_1 - \frac{c_{21}^{(r(t))}Y_1}{m^{(r(t))} + X_2} - c_{22}^{(r(t))}Y_2\right) \end{aligned}$$

$$
\begin{aligned}
&+\frac{\eta\sigma_1^{2(r(t))}}{2}+\psi_3(Y_2-1)\left(-d_2^{(r(t))}-h_2^{(r(t))}Y_2+n_2^{(r(t))}c_{12}^{(r(t))}X_1+\theta_2^{(r(t))}c_{22}^{(r(t))}X_2-f_2^{(r(t))}Y_1\right)\\
&+\frac{\psi_1\sigma_2^{2(r(t))}}{2}+\frac{\psi_2\sigma_3^{2(r(t))}}{2}+\frac{\psi_3\sigma_4^{2(r(t))}}{2}\\
=\;&-b_{11}^{(r(t))}X_1^2-\psi_1h_1Y_1^2-\psi_2b_{22}^{(r(t))}X_2^2-\psi_3h_2Y_2^2+\left(-b_{12}^{(r(t))}-\psi_2b_{21}^{(r(t))}\right)X_1X_2-\left(\psi_2-\psi_3\theta_2^{(r(t))}\right)c_{22}^{(r(t))}X_2Y_2\\
&+\left(-c_{12}^{(r(t))}+\psi_3n_2^{(r(t))}c_{12}^{(r(t))}\right)X_1Y_2+\frac{\left(-\psi_2+\psi_1\theta_1^{(r(t))}\right)c_{21}^{(r(t))}X_2Y_1}{m^{(r(t))}+X_2}+\left(-c_{11}^{(r(t))}+\psi_1n_1^{(r(t))}c_{11}^{(r(t))}\right)X_1Y_1\\
&-\left(\psi_1f_1^{(r(t))}+\psi_3f_2^{(r(t))}\right)Y_1Y_2+\left[a_1^{(r(t))}+\eta b_{11}^{(r(t))}+\psi_2b_{21}^{(r(t))}-\psi_1n_1^{(r(t))}c_{11}^{(r(t))}-\psi_3n_2^{(r(t))}c_{12}^{(r(t))}\right]X_1\\
&+\left[\eta b_{12}^{(r(t))}+\psi_2a_2^{(r(t))}+\psi_2b_{22}^{(r(t))}-\psi_3\theta_2^{(r(t))}c_{22}^{(r(t))}\right]X_2+\left[\eta c_{11}^{(r(t))}+\psi_1h_1^{(r(t))}+\psi_3f_2^{(r(t))}-\psi_1d_1^{(r(t))}\right]Y_1\\
&+\left[\psi_3h_2^{(r(t))}+\eta c_{12}^{(r(t))}+\psi_2c_{22}^{(r(t))}+\psi_1f_1^{(r(t))}-\psi_3d_2^{(r(t))}\right]Y_2-\frac{\psi_1\theta_1^{(r(t))}c_{21}^{(r(t))}X_2}{m^{(r(t))}+X_2}+\frac{\psi_2c_{21}^{(r(t))}Y_1}{m^{(r(t))}+X_2}\\
&+\frac{\eta\sigma_1^{2(r(t))}}{2}\frac{\psi_1\sigma_2^{2(r(t))}}{2}+\frac{\psi_2\sigma_3^{2(r(t))}}{2}+\frac{\psi_3\sigma_4^{2(r(t))}}{2}-\eta a_1^{(r(t))}-\psi_2a_2^{(r(t))}+\psi_1d_1^{(r(t))}+\psi_3d_2^{(r(t))}.
\end{aligned}
\tag{18}
$$

Choose $\psi_1=\min\left\{\frac{1}{n_1^{(r(t))}},\frac{\psi_2}{\theta_1^{(r(t))}}\right\}$ and $\psi_3=\min\left\{\frac{1}{n_2^{(r(t))}},\frac{\psi_2}{\theta_2^{(r(t))}}\right\}$, such that

$$
\begin{aligned}
\mathcal{L}V\le\;&\sup_{X_1>0}\left\{-b_{11}^{(r(t))}X_1^2+\left(a_1^{(r(t))}+\eta b_{11}^{(r(t))}+\psi_2b_{21}^{(r(t))}\right)X_1\right\}\\
&+\sup_{Y_1>0}\left\{-\psi_1h_1^{(r(t))}Y_1^2+\left(\psi_1h_1^{(r(t))}+\eta c_{11}^{(r(t))}+\psi_3f_2^{(r(t))}+\frac{\psi_2c_{21}^{(r(t))}}{m^{(r(t))}}\right)Y_1\right\}\\
&+\sup_{X_2>0}\left\{-\psi_2b_{22}^{(r(t))}X_2^2+\left(\eta b_{12}^{(r(t))}+\psi_2a_2^{(r(t))}+\psi_2b_{22}^{(r(t))}\right)X_2\right\}\\
&+\sup_{Y_2>0}\left\{-\psi_3h_2^{(r(t))}Y_2^2+\left(\psi_3h_2^{(r(t))}+\eta c_{12}^{(r(t))}+\psi_2c_{22}^{(r(t))}+\psi_1f_1^{(r(t))}\right)Y_2\right\}\\
&+\psi_1d_1^{(r(t))}+\psi_3d_2^{(r(t))}+\frac{\eta\sigma_1^{2(r(t))}}{2}+\frac{\psi_1\sigma_2^{2(r(t))}}{2}+\frac{\psi_2\sigma_3^{2(r(t))}}{2}+\frac{\psi_3\sigma_4^{2(r(t))}}{2}.
\end{aligned}
\tag{19}
$$

Setting $\eta=\psi_2=1$, we have

$$
\begin{aligned}
\mathcal{L}V\le\;&\frac{\left(a_1^{(r(t))}+b_{11}^{(r(t))}+b_{21}^{(r(t))}\right)^2}{4b_{11}^{(r(t))}}+\frac{\left(\psi_1h_1^{(r(t))}+c_{11}^{(r(t))}+\psi_3f_2^{(r(t))}+\frac{c_{21}^{(r(t))}}{m^{(r(t))}}\right)^2}{4\psi_1h_1^{(r(t))}}+\frac{\left(a_2^{(r(t))}+b_{12}^{(r(t))}+b_{22}^{(r(t))}\right)^2}{4b_{22}^{(r(t))}}\\
&+\frac{\left(\psi_3h_2^{(r(t))}+c_{12}^{(r(t))}+c_{22}^{(r(t))}+\psi_1f_1^{(r(t))}\right)^2}{4\psi_3h_2^{(r(t))}}+\psi_1d_1^{(r(t))}+\psi_3d_2^{(r(t))}\\
&+\frac{\sigma_1^{2(r(t))}}{2}+\frac{\psi_1\sigma_2^{2(r(t))}}{2}+\frac{\sigma_3^{2(r(t))}}{2}+\frac{\psi_3\sigma_4^{2(r(t))}}{2}:=K_0,
\end{aligned}
\tag{20}
$$

where K_0 is a positive constant. Following the same procedure as in the proof of Theorem 1 by Liu *et al.*,[30] the remaining details are omitted.

Consequently, for any initial value $(X_1(0),Y_1(0),X_2(0),Y_2(0),r(0))\in\mathbb{R}_+^4\times\mathbb{S}$, system (1) admits a unique global solution almost surely. To illustrate this theoretical result, we consider a numerical example involving a two-state switching environment. Specifically, we define the state space as $\mathbb{S}=\{1,2\}$, with transition rates $\gamma_{12}=5$ and $\gamma_{21}=10$. Then the corresponding transition matrix Γ is given by

$$
\Gamma=\begin{bmatrix}\gamma_{11}&\gamma_{12}\\ \gamma_{21}&\gamma_{22}\end{bmatrix}=\begin{bmatrix}-\gamma_{12}&\gamma_{12}\\ \gamma_{21}&-\gamma_{21}\end{bmatrix}=\begin{bmatrix}-5&5\\ 10&-10\end{bmatrix}.
\tag{21}
$$

Note that for a two-state Markov switching, the diagonal elements are completely determined by the off-diagonal transition rates (rows sum to zero). Therefore, in all subsequent analyses of two-state switched systems, we only need to specify the transition rates γ_{12} and γ_{21} to fully characterize the environmental switching dynamics.

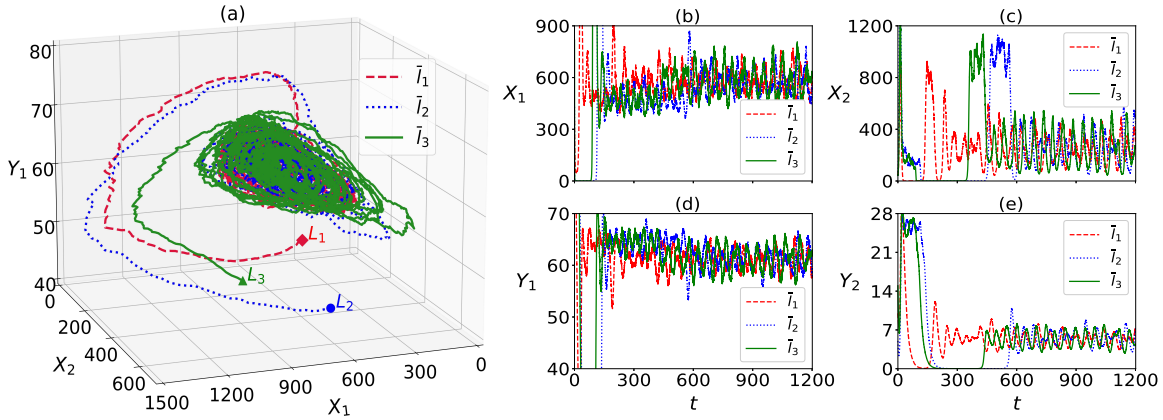


Fig. 5. Trajectories of system (1) with both white noise and Markov switching starting from three initial values L_k $(k = 1,2,3)$. The curves $\bar{I}_k$ represent the trajectories originating from L_k, which eventually oscillate around the equilibrium E^*. Noise and switching cause the stochastic trajectories to fluctuate around the deterministic ones (Fig. 2), with species pair (X_1, Y_1) exhibiting larger fluctuations.

Next, the system is assumed to switch between two environmental states, which are used for numerical illustration rather than to represent a specific ecosystem. State $r(t) = 1$ can be interpreted as a relatively favorable or less disturbed state, such as a resource-rich season or a stable habitat condition. The parameter values are adopted from Ref. [24], specifically: $a_1^{(1)} = 0.85$, $a_2^{(1)} = 0.7$, $b_{11}^{(1)} = 1.4\times10^{-4}$, $b_{22}^{(1)} = 3.5\times10^{-4}$, $c_{11}^{(1)} = 0.013$, $c_{22}^{(1)} = 0.03$, $m^{(1)} = 1200$, $d_1^{(1)} = 0.04$, $d_2^{(1)} = 0.03$, $n_1^{(1)} = 0.007$, $n_2^{(1)} = 0.001$, $\theta_1^{(1)} = 0.0104$, $\theta_2^{(1)} = 0.0093$, $c_{12}^{(1)} = 0.005$, $c_{21}^{(1)} = 0.002$, $b_{12}^{(1)} = 1\times10^{-6}$, $b_{21}^{(1)} = 9\times10^{-4}$, $f_1^{(1)} = 0.002$, $f_2^{(1)} = 5\times10^{-4}$, $h_1^{(1)} = 1.2\times10^{-5}$, $h_2^{(1)} = 1\times10^{-5}$. State $r(t) = 2$ represents an alternative state with changed resource availability, predator activity, and disturbance intensity, such as seasonal stress, habitat degradation, or human interference. The differences in the parameters between the two states reflect reasonable variations in the values of parameters such as growth rate and capture efficiency. The corresponding parameter values are: $a_1^{(2)} = 0.8$, $a_2^{(2)} = 0.78$, $b_{11}^{(2)} = 1\times10^{-4}$, $b_{22}^{(2)} = 3\times10^{-4}$, $c_{11}^{(2)} = 0.01$, $c_{22}^{(2)} = 0.02$, $m^{(2)} = 1200$, $d_1^{(2)} = 0.03$, $d_2^{(2)} = 0.04$, $n_1^{(2)} = 0.006$, $n_2^{(2)} = 0.0005$, $\theta_1^{(2)} = 0.01$, $\theta_2^{(2)} = 0.009$, $c_{12}^{(2)} = 0.004$, $c_{21}^{(2)} = 0.003$, $b_{12}^{(2)} = 1.1\times10^{-6}$, $b_{21}^{(2)} = 8\times10^{-4}$, $f_1^{(2)} = 0.001$, $f_2^{(2)} = 4\times10^{-4}$, $h_1^{(2)} = 1.3\times10^{-5}$, $h_2^{(2)} = 1.1\times10^{-5}$. In particular, throughout the simulation, we assume uniform noise intensities in both states: $\sigma_i^{(1)} = \sigma_i^{(2)} = \sigma$ $(i = 1,2,3,4)$. The corresponding results are presented in Fig. 5.

Figure 5 displays the transient solution trajectories of the system (1) subject to both white noise ($\sigma = 0.005$) and Markov switching. In contrast to the deterministic trajectories (Fig. 2) that converge to the positive equilibrium E^*, the stochastic trajectories fluctuate around their deterministic counterparts due to environmental stochasticity and Markov switching, reflecting how natural populations rarely achieve perfect equilibrium in variable environments. This oscillation phenomenon is particularly evident for the species pair (X_1, Y_1) rather than the pair (X_2, Y_2). It may be because predator Y_1 obtains resources from both X_1 and X_2, and its interaction with X_2 follows a Holling type II functional response. The analysis indicates that low-intensity noise mainly causes minor fluctuations in the solutions while still maintaining the tendency towards a stable steady state.

4.2. Effects of coupling strengths under Gaussian white noise

In this subsection, the influence of coupling strength on the system (1) subjected to white noise perturbation will be analyzed. As shown in Fig. 5, the stochastic solution trajectories exhibit highly irregular oscillations, making it difficult for the phase diagram and time series to provide meaningful dynamical information. Therefore, we introduce the stationary probability density function and the most probable trajectory as analytical tools for the stochastic part.

Definition 1[31,32] The probability distribution of random variable X is described by its probability density function $p(X)$. The stationary probability density function (SPDF), denoted as $p_s(X)$, is defined for a stochastic process whose probability density function remains time-invariant, i.e., $\partial p_s(X)/\partial t = 0$.

Definition 2[33–35] The most probable trajectory $X_m(t)$ is defined as the continuous path that passes through local maxima of the probability density function $p(X,t)$ at each time point t. Mathematically, $X_m(t)$ satisfies

$$\nabla_X p(X,t)|_{X=X_m} = 0, \tag{22}$$

with the Hessian matrix $\nabla_X^2 p(X,t)|_{X=X_m}$ being negative definite.

Using $Y_1(t)$ as our focal variable, we define Y_{1m} as the local maximum point of the $p_s(Y_1)$, representing the most probable stationary solution (MPSS) of Y_1 in stochastic system (1). Similar to the analysis of the deterministic non-switched system shown in Fig. 3, Fig. 6 depicts how Y_{1m} varies with coupling strength c_{21}, allowing a direct comparison between deterministic and stochastic bifurcation behaviors in the non-switched case.

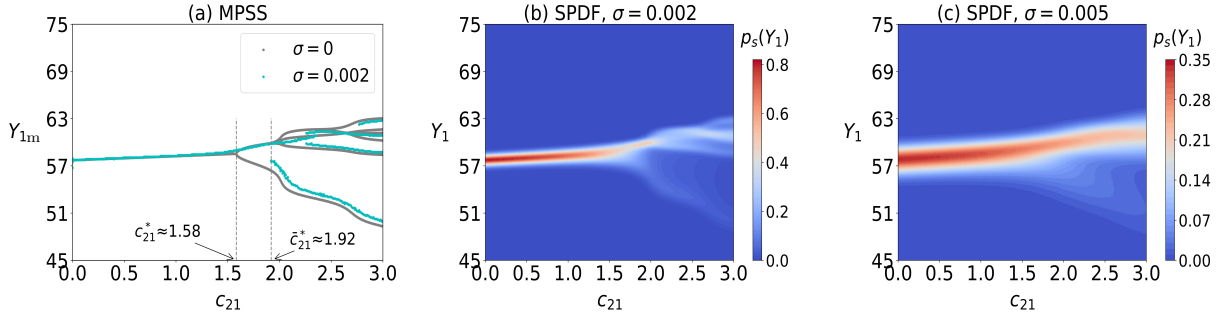


Fig. 6. Bifurcation diagrams of the stationary distribution in the stochastic non-switched system with varying coupling strengths c_{21}. (a) Bifurcation diagram of MPSS $Y_{1\mathrm{m}}$ versus c_{21} for case $\sigma = 0$ and $\sigma = 0.002$. $c_{21}^* \approx 1.58$ denotes the Andronov–Hopf bifurcation value, while $\tilde{c}_{21}^* \approx 1.92$ represents the stochastic P-bifurcation value. (b), (c) Marginal SPDFs $p_{\mathrm{s}}(Y_1)$ projected onto the c_{21}–Y_1 plane for noise intensities $\sigma = 0.002$ or $\sigma = 0.005$, demonstrating that increasing noise intensity causes reduced $p_{\mathrm{s}}(Y_1)$ value and fewer peaks.

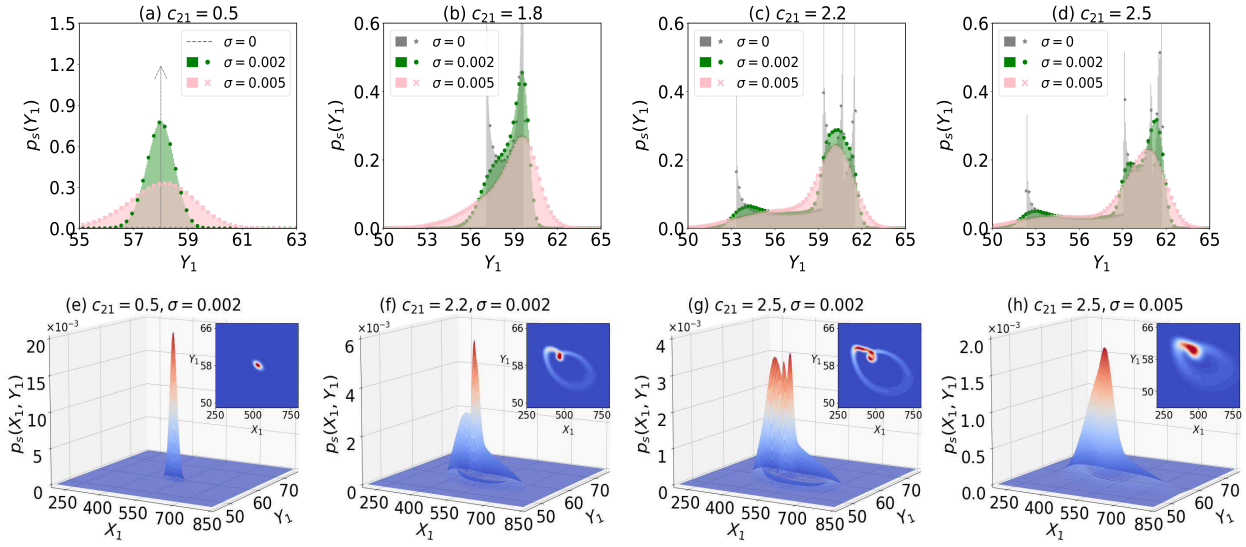


Fig. 7. Marginal and joint SPDFs under varying coupling strengths c_{21} and noise intensities σ. (a)–(d) illustrate the evolution of $p_{\mathrm{s}}(Y_1)$ from unimodal to multimodal distributions, demonstrating that increased noise intensity suppresses complex multimodal oscillations but broadens the distribution. Vertical arrows mark the equilibrium position in (a), indicating $p_{\mathrm{s}}(Y_1) \to \infty$. (e)–(h) present three-dimensional views illustrating the transition from unimodal to multimodal distributions.

Figure 6 presents the bifurcation behavior of stationary distributions in the stochastic two-predator two-prey system as coupling strength c_{21} varies. Figure 6(a) compares the deterministic non-switched system with the stochastic non-switched system. The deterministic case exhibits a smooth and continuous Andronov–Hopf bifurcation at $c_{21} \approx 1.58$, whereas the stochastic case remains a unimodal distribution until $c_{21} \approx 1.92$. This occurs because environmental noise diffuses lower-probability peaks (see Fig. 6(b)) and delays the onset of the bifurcation phenomenon. Only when the coupling strength increases sufficiently ($c_{21} \approx 1.92$) does the underlying deterministic bifurcation structure overcome the diffusive effect of noise, allowing $p_{\mathrm{s}}(Y_1)$ to transition from unimodal to bimodal through a stochastic P-bifurcation.

Additionally, at $\sigma = 0.002$, MPSS $Y_{1\mathrm{m}}$ exhibits a narrower range with fewer peaks, demonstrating noise-induced suppression of extreme fluctuations and multimodal oscillations. Figures 6(b) and 6(c) further display the $p_{\mathrm{s}}(Y_1)$ for different noise intensities ($\sigma = 0.002$ and $\sigma = 0.005$). At $\sigma = 0.002$, the $p_{\mathrm{s}}(Y_1)$ evolves from unimodal to bimodal or multimodal states, with higher probability density at higher Y_1 values, indicating preferential stabilization at higher predator populations. However, at $\sigma = 0.005$, although the complex multimodal patterns are replaced by simplified unimodal distributions, the significantly widened distribution range indicates reduced ecosystem stability as intense environmental fluctuations eliminate alternative stable distributions.

Figure 7 further shows the marginal stationary probability density function $p_{\mathrm{s}}(Y_1)$ and joint stationary probability density function $p_{\mathrm{s}}(X_1, Y_1)$ under the combined effects of varying coupling and noise. At weak coupling ($c_{21} = 0.5$), $p_{\mathrm{s}}(Y_1)$ remains unimodal regardless of noise intensity. At intermediate coupling ($c_{21} = 1.8$), the deterministic non-switched system develops two peaks, but increasing noise eliminates the lower peak while broadening the dominant one. At strong coupling ($c_{21} = 2.2$ or 2.5), noise progressively simplifies the multimodal deterministic structure, merging adjacent peaks and diffusing the trajectory range. Hence, Figs. 7(a)–7(d) validate the stochastic P-bifurcations through unimodal-to-multimodal transitions, while Figs. 7(e)–7(h) visually reveal the evolution

from needle-like equilibria to broad multimodal oscillations. Figures 7(g) and 7(h) further reveal that noise intensity can smooth complex coupling-induced structures into dispersed distributions, reduce peak values, and consequently weaken system stability.

4.3. Effects of coupling strengths under Gaussian white noise and Markov switching

The previous section explored the influence of white noise on the stationary distribution of the system in a single environmental state. However, due to factors such as seasonal changes and human hunting, the interaction parameters among populations are not constant. Markov switching is used to reflect the impact of heterogeneous environments on population dynamics. Since the occurrence of switching is accompanied by at least two pairs of system parameters, the coupling effect in the switched system requires the analysis of at least two coupling parameters simultaneously. Next, we study the combined influence of continuous fluctuations (white noise) and discrete environmental shifts (Markov switching) on system (1).

In this framework, we focus on the scenario where the coupling strength alternates between two environmental states, i.e., $\mathbb{S} = \{1,2\}$. Accordingly, the coupling strength is $c_{21}^{(1)}$ at state $r(t) = 1$ and switches to $c_{21}^{(2)}$ at state $r(t) = 2$. To quantitatively characterize the bifurcation dynamics under this switching effect, we introduce an indicator $N_{Y_{1\mathrm{m}}}$, defined as the number of local maximum points $Y_{1\mathrm{m}}$ in the stationary probability density function $p_{\mathrm{s}}(Y_1)$ of species Y_1. Topologically, $N_{Y_{1\mathrm{m}}} = 1$ corresponds to a unimodal distribution, whereas $N_{Y_{1\mathrm{m}}} = 2$ signifies a bimodal distribution.

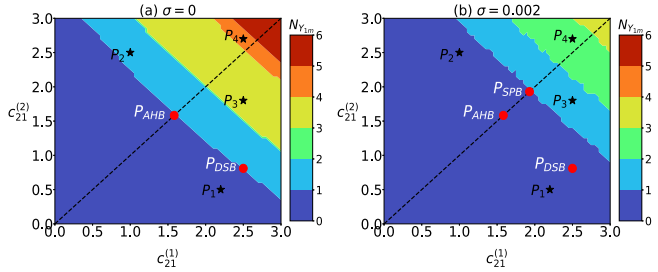


Fig. 8. Bifurcation diagrams in the coupling strengths $c_{21}^{(1)}$–$c_{21}^{(2)}$ plane quantifying the number $N_{Y_{1\mathrm{m}}}$ of peaks with fixed transition rates $\gamma_{12} = \gamma_{21} = 5$. (a) depicts the deterministic case and (b) the stochastic case with different $c_{21}^{(1)}$ and $c_{21}^{(2)}$. Here, P_{AHB} is the Andronov–Hopf bifurcation point, P_{SPB} is the stochastic P-bifurcation point, and P_{DSB} is the bifurcation point of the noise-free switched system. White noise elevates the critical threshold of coupling-induced oscillations under fixed transition rates.

Figure 8 displays the bifurcation behavior of the system (1) under fixed transition rates and varying switching parameters. Unlike the single-parameter bifurcation diagrams (Figs. 3 and 6), the proposed method quantifies and compares the stationary responses of the stochastic switched system from the perspective of the most probable trajectory using $N_{Y_{1\mathrm{m}}}$. Along the black diagonal line $c_{21}^{(1)} = c_{21}^{(2)}$, the system effectively has no switching effects. Consequently, the system recovers the non-switching baseline where critical thresholds $P_{\mathrm{AHB}} = (c_{21}^*, c_{21}^*) = (1.58, 1.58)$ and $P_{\mathrm{SPB}} = (\bar{c}_{21}^*, \bar{c}_{21}^*) = (1.92, 1.92)$ align with the single-state bifurcations identified in Figs. 3 and 6. Outside the diagonal region where switching occurs (modeling natural heterogeneity across habitats or seasons), the bifurcation thresholds depend on combined parameters of all subsystems rather than a single bifurcation value c_{21}^* or $\bar{c}_{21}^*$. Specifically, the points on the boundary curves between differently colored regions represent the critical transition values of the switched system. While deterministic non-switched systems lose unimodal stability at $c_{21} > c_{21}^* \approx 1.58$, the switched system maintains unimodality even at $c_{21} > c_{21}^*$, demonstrating how Markov switching weakens coupling-induced multimodal oscillations. For instance, the point $P_{\mathrm{DSB}} = (c_{21}^{(1)}, c_{21}^{(2)}) = (2.5, 0.81)$ in Fig. 8(a) represents the bifurcation point at which the $p_{\mathrm{s}}(Y_1)$ transitions from a unimodal form ($N_{Y_{1\mathrm{m}}} = 1$) to a bimodal form ($N_{Y_{1\mathrm{m}}} = 2$). Compared with Fig. 8(a), white noise ($\sigma = 0.002$) in Fig. 8(b) shifts the boundaries between colored regions toward the upper right, causing the $N_{Y_{1\mathrm{m}}}$ values to remain unchanged or decrease. This indicates that noise influences the system similarly regardless of parameter switching. These results also suggest that Markov switching more effectively elevates bifurcation thresholds and suppresses complex cascading bifurcation phenomena, highlighting the conservation importance of preserving environmental heterogeneity.

In Fig. 8, we select four characteristic points P_i ($i = 1,2,3,4$) from the $c_{21}^{(1)}$–$c_{21}^{(2)}$ plane for detailed analysis and plot their $p_{\mathrm{s}}(Y_1)$ in Fig. 9. Under fixed transition rates $\gamma_{12} = \gamma_{21} = 5$, the $p_{\mathrm{s}}(Y_1)$ exhibits varying multimodal characteristics across different points: At P_1, the system maintains a unimodal distribution ($N_{Y_{1\mathrm{m}}} = 1$) for both noise intensities $\sigma = 0$ and $\sigma = 0.002$; at P_2, it transitions to bimodality when $\sigma = 0$ ($N_{Y_{1\mathrm{m}}} = 2$) while remaining unimodal when $\sigma = 0.002$ ($N_{Y_{1\mathrm{m}}} = 1$); at P_3, the distribution becomes more complex with a quadrimodal distribution for $\sigma = 0$ ($N_{Y_{1\mathrm{m}}} = 4$) and bimodal distribution for $\sigma = 0.002$ ($N_{Y_{1\mathrm{m}}} = 2$); finally, at P_4, the system shows five peaks when $\sigma = 0$ ($N_{Y_{1\mathrm{m}}} = 5$) but stabilizes into a trimodal distribution ($N_{Y_{1\mathrm{m}}} = 3$) when $\sigma = 0.002$, demonstrating how environmental states interact with system parameters to shape population stability patterns. Therefore, Fig. 9 reveals how environmental switching shapes the peak structure of $p_{\mathrm{s}}(Y_1)$ under white noise, demonstrating how environmental heterogeneity can help prevent species collapse in homogeneous environments.

Figure 10 displays the bifurcation behavior of the system under the fixed switching parameters and varying transition rates. The points on the γ_{12}–γ_{21} plane, such as $\gamma_{12} = 3$ and $\gamma_{21} = 8$, represent the transition rate from state $r(t) = 1$ to state $r(t) = 2$ as 3, and the reverse transition rate as 8. In Fig. 6(a), the deterministic non-switched system shows a

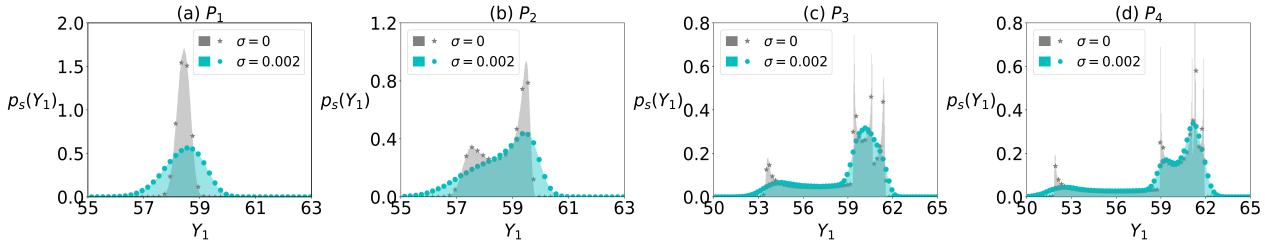


Fig. 9. Marginal SPDFs $p_s(Y_1)$ at switching parameter points P_i $(i = 1,2,3,4)$, validating the topological transition from unimodal to multimodal distributions. Here, $P_1 = (2.2, 0.5)$, $P_2 = (1, 2.5)$, $P_3 = (2.5, 1.8)$, and $P_4 = (2.5, 2.7)$. White noise weakens coupling-induced multimodal oscillations.

multi-peak stationary distribution at $c_{21} = 3$ and $N_{Y_{1m}} = 6$. After Markov switching is introduced, $N_{Y_{1m}}$ decreases to 2 at $c_{21}^{(1)} = 0.5$ and $c_{21}^{(2)} = 3$ in Figs. 8(a) and 10(a). This suggests that Markov switching weakens multi-peak population oscillations and raises the threshold for coupling-induced oscillation. It is worth noting that when both γ_{12} and γ_{21} are large (indicating rapid environmental switching), values of $N_{Y_{1m}}$ and the parameter region corresponding to $N_{Y_{1m}} > 4$ are smaller, demonstrating that faster switching effectively suppresses multimodal oscillations and reduces the probability of extreme states. In particular, with γ_{21} fixed (e.g., $\gamma_{21} = 3$), increasing γ_{12} transforms the $p_s(Y_1)$ from unimodal ($N_{Y_{1m}} = 1$) to bimodal ($N_{Y_{1m}} = 2$) to quadrimodal ($N_{Y_{1m}} = 4$), exhibiting a period-doubling-like bifurcation pattern arising from environmental heterogeneity and state-switching dynamics. Compared to Fig. 10(a), the $N_{Y_{1m}}$ values in regions influenced by white noise ($\sigma = 0.002$) in Fig. 10(b) remain unchanged or decrease. Thus, the suppressing effect of white noise on coupling-induced bifurcation also persists in the switched system.

Similar to Fig. 9, we select four specific points Q_i $(i = 1,2,3,4)$ in Fig. 10 to correspond to four sets of different transition rates. The corresponding marginal stationary probability density functions $p_s(Y_1)$ are given in Fig. 11. Figure 11 illustrates the evolution of the $p_s(Y_1)$ at points Q_1–Q_4 under increasing noise intensity with peak numbers reducing from $N_{Y_{1m}} = 2$ to $N_{Y_{1m}} = 1$ at Q_1, $N_{Y_{1m}} = 4$ to $N_{Y_{1m}} = 2$ at Q_2, $N_{Y_{1m}} = 4$ to $N_{Y_{1m}} = 3$ at Q_3, and $N_{Y_{1m}} = 6$ to $N_{Y_{1m}} = 4$ at Q_4. In conclusion, environmental noise and Markov switching can weaken the multimodal phenomenon caused by coupling, thereby simplifying the system dynamics.

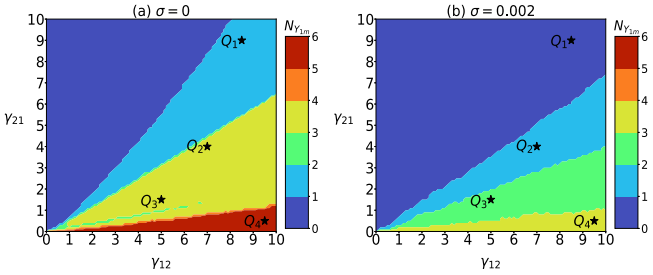


Fig. 10. Bifurcation diagrams in the transition rates γ_{12}–γ_{21} plane quantifying the number $N_{Y_{1m}}$ of peaks with fixed switching parameters $c_{21}^{(1)} = 0.5$ and $c_{21}^{(2)} = 3$. (a) depicts the deterministic case and (b) the stochastic case with different γ_{12} and γ_{21}. The $N_{Y_{1m}}$ values influenced by white noise in (b) remain unchanged or decrease compared to (a). Markov switching elevates the threshold for coupling-induced oscillations under fixed coupling strengths.

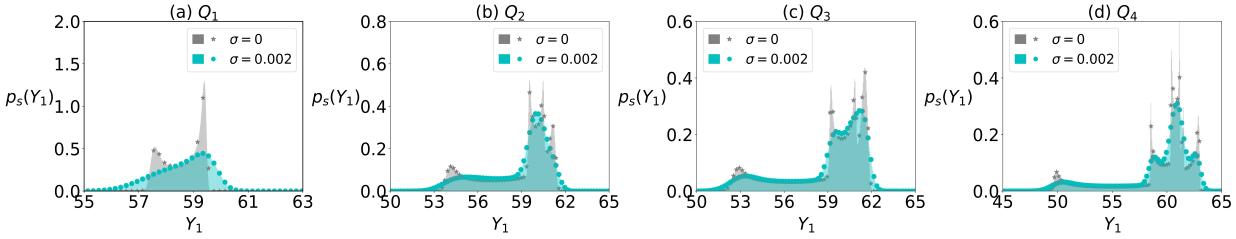


Fig. 11. Marginal SPDFs $p_s(Y_1)$ at different transition rate points Q_i $(i = 1,2,3,4)$, validating the topological transition from unimodal to multimodal distributions. Here, $Q_1 = (8.5, 9)$, $Q_2 = (7, 4)$, $Q_3 = (5, 1.5)$, $Q_4 = (9.5, 0.5)$. Markov switching has an effect similar to that of white noise and tends to suppress coupling-induced multimodal behavior.

5. Conclusion

We analyze a four-dimensional two-predator two-prey system with coupling, Gaussian white noise, and Markov switching, and examine how these factors jointly shape bifurcation thresholds and species coexistence.

Compared with existing two-dimensional predator–prey models with Markov switching, this model extends the analysis from a single predator–prey interaction to two coupled predator–prey pairs. It can describe inter-prey competition, inter-predator competition, cross predation, and asymmetric functional responses. Thus, the effects of coupling strength on multispecies coexistence can be analyzed more explicitly. In addition, this work focuses on the joint influence of coupling strength, Gaussian white noise, and Markov switching on bifurcation behavior.

The coupling-induced bifurcation mechanism is examined under deterministic and stochastic conditions. In the deterministic non-switched case, increasing the coupling

strength induces an Andronov–Hopf bifurcation. The system changes from a stable coexistence equilibrium to periodic or multimodal oscillations. Biologically, stronger coupling enhances cross predation, modifies trophic interactions, and destabilizes the corresponding predator–prey pair. The effects of Gaussian white noise and Markov switching are characterized using stationary probability density functions and most probable trajectories. Weak noise delays stochastic P-bifurcation and reduces the number of peaks in the stationary distribution. Markov switching also suppresses coupling-induced multimodal oscillations under alternating environmental states. These results suggest that environmental switching can buffer strong coupling effects and weaken extreme oscillatory states. For the switched system, bifurcation behavior depends on parameters from different environmental states and their transition rates. A single critical value is therefore insufficient. An indicator based on the most probable trajectory is introduced to quantify the number of local maxima in the stationary distribution. It distinguishes unimodal, bimodal, and multimodal stationary responses. Overall, the results show that Gaussian white noise and Markov switching reshape the effects of coupling on stationary distributions and provide theoretical insight into species coexistence in switching environments.

Further work will consider spatial coupling, more general functional responses, and additional noise structures relevant to fragmented habitats.

Appendix A: Linearization of the two-predator two-prey system

To analyze the local stability of the interior equilibrium $E^*(x_1^*,y_1^*,x_2^*,y_2^*)$ of the deterministic non-switched system (1), we employ the linearization method and characteristic equation analysis. First, we introduce centered variables to transform the system state into the interior equilibrium, eliminate the constant terms, and simplify the linearization process. Define

$$\begin{aligned} U_1 &= x_1 - x_1^*, \quad V_1 = y_1 - y_1^*, \\ U_2 &= x_2 - x_2^*, \quad V_2 = y_2 - y_2^*, \end{aligned} \tag{A1}$$

where U_1,V_1,U_2,V_2 represent small perturbations around x_1^*,y_1^*,x_2^*,y_2^* (i.e., $|U_1| \ll x_1^*$, $|V_1| \ll y_1^*$, $|U_2| \ll x_2^*$, $|V_2| \ll y_2^*$). Substituting transformation Eq. (A1) into the deterministic part of system (1), the right-hand side of each equation is expanded by Taylor expansion near the positive equilibrium, while fourth-order and higher-order terms are neglected. Taking $x_1 = x_1^* + U_1$ as an example, substituting it into the deterministic part of system (1) gives

$$\begin{aligned} \frac{\mathrm{d}U_1}{\mathrm{d}t} &= \frac{\mathrm{d}(x_1^*+U_1)}{\mathrm{d}t} = \frac{\mathrm{d}x_1}{\mathrm{d}t} \\ &= a_1(x_1^*+U_1) - b_{11}(x_1^*+U_1)^2 - b_{12}(x_1^*+U_1)(x_2^*+U_2) \\ &\quad -c_{11}(x_1^*+U_1)(y_1^*+V_1) - c_{12}(x_1^*+U_1)(y_2^*+V_2) \\ &= a_1x_1^* - b_{11}x_1^{*2} - b_{12}x_1^*x_2^* - c_{11}x_1^*y_1^* - c_{12}x_1^*y_2^* \\ &\quad +(a_1 - 2b_{11}x_1^* - b_{12}x_2^* - c_{11}y_1^* - c_{12}y_2^*)U_1 \\ &\quad -b_{12}x_1^*U_2 - c_{11}x_1^*V_1 - c_{12}x_1^*V_2 - b_{11}U_1^2 \\ &\quad -b_{12}U_1U_2 - c_{11}U_1V_1 - c_{12}U_1V_2 \\ &= (a_1 - 2b_{11}x_1^* - b_{12}x_2^* - c_{11}y_1^* - c_{12}y_2^*)U_1 \\ &\quad -c_{11}x_1^*V_1 - b_{12}x_1^*U_2 - c_{12}x_1^*V_2 \\ &\quad -b_{11}U_1^2 - b_{12}U_1U_2 - c_{11}U_1V_1 - c_{12}U_1V_2. \end{aligned} \tag{A2}$$

While the variable $\dot{x}_2$ contains a fractional term $g(x_2,y_1) = \frac{x_2y_1}{m+x_2}$, substitute $y_1 = y_1^* + V_1, x_2 = x_2^* + U_2$ and expand $\frac{(x_2^*+U_2)(y_1^*+V_1)}{(m+x_2^*+U_2)}$ around $x_2 = x_2^*$ and $y_1 = y_1^*$ retaining terms up to the third order. We can obtain

$$\begin{aligned} \bar{g}(x_2,y_1) \approx\ & \frac{x_2^*y_1^*}{m+x_2^*} + \frac{my_1^*}{(m+x_2^*)^2}U_2 + \frac{x_2^*}{m+x_2^*}V_1 \\ & -\frac{my_1^*}{(m+x_2^*)^3}U_2^2 + \frac{m}{(m+x_2^*)^2}U_2V_1 \\ & +\frac{my_1^*}{(m+x_2^*)^4}U_2^3 - \frac{m}{(m+x_2^*)^3}U_2^2V_1. \end{aligned} \tag{A3}$$

Following the same procedure as for Eq. (A2), we obtain

$$\begin{aligned} \frac{\mathrm{d}V_1}{\mathrm{d}t} \approx\ & n_1c_{11}y_1^*U_1 + \Big(-d_1 - 2h_1y_1^* + n_1c_{11}x_1^* + \frac{\theta_1c_{21}x_2^*}{m+x_2^*} \\ & -f_1y_2^*\Big)V_1 + \frac{\theta_1c_{21}my_1^*}{(m+x_2^*)^2}U_2 - f_1y_1^*V_2 \\ & -h_1V_1^2 + n_1c_{11}U_1V_1 - f_1V_1V_2 + \theta_1c_{21}\Theta, \\ \frac{\mathrm{d}U_2}{\mathrm{d}t} \approx\ & -b_{21}x_2^*U_1 - \frac{c_{21}x_2^*}{m+x_2^*}V_1 + \Big(a_2 - 2b_{22}x_2^* - b_{21}x_1^* \\ & -\frac{c_{21}my_1^*}{(m+x_2^*)^2} - c_{22}y_2^*\Big)U_2 - c_{22}x_2^*V_2 \\ & -b_{22}U_2^2 - b_{21}U_1U_2 - c_{22}U_2V_2 - c_{21}\Theta, \end{aligned} \tag{A4}$$

$$\begin{aligned} \frac{\mathrm{d}V_2}{\mathrm{d}t} =\ & n_2c_{12}y_2^*U_1 - f_2y_2^*V_1 + \theta_2c_{22}y_2^*U_2 \\ & +(-d_2 - 2h_2y_2^* + n_2c_{12}x_1^* + \theta_2c_{22}x_2^* - f_2y_1^*)V_2 \\ & -h_2V_2^2 + n_2c_{12}U_1V_2 + \theta_2c_{22}U_2V_2 - f_2V_1V_2, \end{aligned} \tag{A5}$$

where

$$\begin{aligned} \Theta =\ & \frac{m}{(m+x_2^*)^2}U_2V_1 - \frac{m}{(m+x_2^*)^3}U_2^2V_1 \\ & -\frac{my_1^*}{(m+x_2^*)^3}U_2^2 + \frac{my_1^*}{(m+x_2^*)^4}U_2^3. \end{aligned} \tag{A6}$$

Therefore, in a neighborhood of the positive equilibrium E^*, after linearizing the deterministic part of system (1), the following perturbation system in matrix form can be obtained:

$$\dot{\boldsymbol{W}} = J(x_1^*, y_1^*, x_2^*, y_2^*)\boldsymbol{W} + \boldsymbol{D}, \tag{A7}$$

where $\boldsymbol{W} = (U_1, V_1, U_2, V_2)^{\mathrm{T}}$ is the perturbation vector, and $J(x_1^*, y_1^*, x_2^*, y_2^*)$ is the Jacobian matrix of the system evaluated at E^*, and $\boldsymbol{D} = (D_1, D_2, D_3, D_4)^{\mathrm{T}}$ is the vector of higher-order residual terms. Following the derivations in Eqs. (A2)–(A6), the Jacobian matrix J can be written as follows:

$$J(x_1, y_1, x_2, y_2) = \begin{bmatrix} J_{11} & J_{12} & J_{13} & J_{14} \\ J_{21} & J_{22} & J_{23} & J_{24} \\ J_{31} & J_{32} & J_{33} & J_{34} \\ J_{41} & J_{42} & J_{43} & J_{44} \end{bmatrix}, \tag{A8}$$

where each element is defined as

$$\begin{aligned}
J_{11} &= a_1 - 2b_{11}x_1 - b_{12}x_2 - c_{11}y_1 - c_{12}y_2,\ J_{12} = -c_{11}x_1,\ J_{13} = -b_{12}x_1,\ J_{14} = -c_{12}x_1,\\
J_{21} &= n_1c_{11}y_1,\ J_{22} = -d_1 - 2h_1y_1 + n_1c_{11}x_1 + \frac{\theta_1c_{21}x_2}{m+x_2} - f_1y_2,\ J_{23} = \frac{\theta_1c_{21}my_1}{(m+x_2)^2},\ J_{24} = -f_1y_1,\\
J_{31} &= -b_{21}x_2,\ J_{32} = -\frac{c_{21}x_2}{m+x_2},\ J_{33} = a_2 - 2b_{22}x_2 - b_{21}x_1 - \frac{mc_{21}y_1}{(m+x_2)^2} - c_{22}y_2,\ J_{34} = -c_{22}x_2,\\
J_{41} &= n_2c_{12}y_2,\ J_{42} = -f_2y_2,\ J_{43} = \theta_2c_{22}y_2,\ J_{44} = -d_2 - 2h_2y_2 + n_2c_{12}x_1 + \theta_2c_{22}x_2 - f_2y_1.
\end{aligned} \tag{A9}$$

According to Eqs. (A2)–(A6), the residual vector $\boldsymbol{D}$, which includes higher-order terms, is given by

$$\begin{aligned}
D_1 &= -b_{11}U_1^2 - b_{12}U_1U_2 - c_{11}U_1V_1 - c_{12}U_1V_2,\\
D_2 &= -h_1V_1^2 + n_1c_{11}U_1V_1 - f_1V_1V_2 + \theta_1c_{21}\Theta,\\
D_3 &= -b_{22}U_2^2 - b_{21}U_1U_2 - c_{22}U_2V_2 - c_{21}\Theta,\\
D_4 &= -h_2V_2^2 + n_2c_{12}U_1V_2 + \theta_2c_{22}U_2V_2 - f_2V_1V_2.
\end{aligned} \tag{A10}$$

Acknowledgment

Project supported by the National Natural Science Foundation of China (Grant No. 12472033).

References

[1] Suzuki S S, Baba Y G and Toju H 2023 *Nat. Ecol. Evol.* **7** 1432
[2] Jin Y F 2015 *Chin. Phys. B* **24** 060502
[3] Alwan M S and Liu X Z 2018 *Theory of Hybrid Systems: Deterministic and Stochastic* (Berlin: Springer-Verlag) p. 2
[4] Lu C 2021 *Math. Comput. Simul.* **181** 316
[5] Zou X L, Lin C, Qian Y and Lv J L 2026 *Math. Comput. Simul.* **240** 270
[6] Liu M 2019 *Nonlinear Dyn.* **96** 417
[7] Liu Q, Jiang D, Hayat T and Alsaedi A 2019 *Physica A* **527** 121264
[8] Xia L, Sun J J, Ying Z G, Huan R H and Zhu W Q 2021 *Appl. Math. Mech.* **42** 1123
[9] Wei W, Xu W, Liu J K, Song Y and Zhang S 2023 *Appl. Math. Model.* **117** 563
[10] Sun Y N, Liu X Z and Lei Y M 2026 *Chin. Phys. B* **35** 010507
[11] Liu M 2024 *J. Math. Anal. Appl.* **535** 128096
[12] Du N H and Nguyen N N 2025 *Nonlinear Anal. Hybrid Syst.* **58** 101621
[13] MacArthur R H 1970 *Theor. Popul. Biol.* **1** 1
[14] May R M 1971 *Math. Biosci.* **12** 59
[15] Takeuchi Y and Adachi N 1984 *Math. Biosci.* **70** 65
[16] Kirlinger G 1986 *Math. Biosci.* **82** 165
[17] Kirlinger G 1989 *Math. Biosci.* **96** 1
[18] Wootton J T and Emmerson M 2005 *Annu. Rev. Ecol. Evol. Syst.* **36** 419
[19] Rong Q N, Zhai Y J, Kang Y M and Liu R N 2025 *Chaos Solitons Fractals* **201** 117181
[20] Stankovski T, Pereira T, McClintock P V E and Stefanovska A 2017 *Rev. Mod. Phys.* **89** 045001
[21] Xiang Z Y and Song X Y 2006 *Chaos Solitons Fractals* **29** 1121
[22] Xiang Z Y, Song X Y and Zhang F Q 2008 *Chaos Solitons Fractals* **37** 424
[23] Mustafin A 2015 *Commun. Nonlinear Sci. Numer. Simul.* **29** 391
[24] Jana A and Roy S K 2021 *Ecol. Complex.* **47** 100942
[25] MacArthur R H 1984 *Geographical Ecology: Patterns in the Distribution of Species* (Princeton: Princeton University Press) p. 40
[26] Sikder A and Roy A B 1993 *Biosystems* **31** 39
[27] Liu M, Peng Y, Ren X J and Zhang J P 2026 *Math. Comput. Simul.* **239** 483
[28] Medvedev G and Yoo Y 2007 *Physica D* **228** 87
[29] Frankel M L, Kovačič G, Roytburd V and Timofeyev I 2000 *Physica D* **137** 295
[30] Liu Q and Jiang D 2019 *Stoch. Anal. Appl.* **37** 321
[31] Zhu W Q and Yang Y Q 1996 *J. Appl. Mech.* **63** 493
[32] Wu D, Peng D H and Wang S L 2024 *Eng. Struct.* **308** 117986
[33] Cheng Z, Duan J Q and Wang L 2016 *Commun. Nonlinear Sci. Numer. Simul.* **30** 108
[34] Han P, Xu W, Wang L and Ma S C 2020 *Chaos Solitons Fractals* **132** 109612
[35] Wang H, Chen X, Yang F and Duan J Q 2025 *Chaos* **35** 053123